



Article

Synthesis of $Zn_xCd_{1-x}Se@ZnO$ Hollow Spheres in Different Sizes for Quantum Dots Sensitized Solar Cells Application

Libo Yu ¹ and Zhen Li ^{1,2,*}

¹ College of Chemistry and Chemical Engineering, Hexi University, Zhangye City 734000, Gansu Province, China; yulibo_665@163.com

² Key Laboratory of Hexi Corridor Resources Utilization of Gansu, Hexi University, Zhangye City 734000, Gansu Province, China

* Correspondence: lizhen_665@163.com

Received: 7 January 2019; Accepted: 18 January 2019; Published: 22 January 2019



Abstract: $Zn_xCd_{1-x}Se@ZnO$ hollow spheres (HS) were successfully fabricated for application in quantum dot sensitized solar cells (QDSSCs) based on ZnO HS through the ion-exchange process. The sizes of the $Zn_xCd_{1-x}Se@ZnO$ HS could be tuned from ~300 nm to ~800 nm using ZnO HS pre-synthesized by different sizes of carbonaceous spheres as templates. The photovoltaic performance of QDSSCs, especially the short-circuit current density (J_{sc}), experienced an obvious change when different sizes of $Zn_xCd_{1-x}Se@ZnO$ HS are employed. The $Zn_xCd_{1-x}Se@ZnO$ HS with an average size distribution of ~500 nm presented a better performance than the QDSSCs based on other sizes of $Zn_xCd_{1-x}Se@ZnO$ HS. When using the mixture of $Zn_xCd_{1-x}Se@ZnO$ HS with different sizes, the power conversion efficiency can be further improved. The size effect of the hollow spheres, light scattering, and composition gradient structure $Zn_xCd_{1-x}Se@ZnO$ HS are responsible for the enhancement of the photovoltaic performance.

Keywords: alloyed quantum dots; hollow spheres; sensitized solar cells; zinc oxide

1. Introduction

The huge consumption of fossil fuels, and global warming caused by worldwide industries, have forced the exploration of clean, environmentally friendly energy [1–3]. Solar energy is one of the best candidates for a future energy source. The common use of solar energy is for various photovoltaic devices including silicon solar cells, thin film solar cells, dye-sensitized solar cells, quantum dots sensitized solar cells, and perovskite solar cells [4–6]. Among them, quantum dot sensitized solar cells (QDSSCs) have become the focus of investigation, because of their intrinsic advantages, including their superior extinction coefficient, possibility of multiple excitons generation, and higher theoretical power conversion efficiency (44%) than semiconductor solar cells, based on the Shockley–Queisser limit (33%) [7–9]. The concept of QDSSCs originated from dye sensitized solar cells (DSSCs), and its configuration and working principle are also similar to DSSCs [10]. The DSSCs consists of three parts, including the photoanode, electrolyte, and counterelectrode, which have been well been developed in the past decade, especially in the building of different types of photoanodes and electrolytes [11–13]. Inspired by the development of DSSCs, the investigation of QDSSCs has also made great achievements in the past years.

The power conversion efficiency of QDSSCs has constantly improved in recent years as a result of research efforts. The most remarkable breakthrough is that a power conversion efficiency of over 10% was achieved using Zn–Cu–In–Se quantum dots based on a TiO_2 film [14,15]. However, there

are still many challenges to be overcome in order to reach the theoretical limit (44%), indicating that the design of QDSSCs has still not been well optimized. As a key part of the photoanode in QDSSCs, the metal oxide particles of ~25 nm are most commonly used because of a high specific surface area for QD loading [16–18]. However, typical metal oxide particles of ~25 nm in the photoanode are weak when generating light scattering, because the size of the particles is far smaller than the wavelength of the visible light, causing a less light harvesting efficiency. Based on the Mie theory and Anderson localization of light [19], the resonant scattering of light is predicted to occur for spherical particles only when the particle size is comparable to the wavelength of the incident light [20]. To tackle this issue, metal oxide hollow spheres seem to be an appropriate choice for application in QDSSCs. Among these hollow structures, ZnO hollow spheres (HS) are particularly attractive as photoanodes for QDSSCs, because of their high electron mobility and low production cost [21]. Moreover, the size of ZnO HS is easy to control during the fabrication process by using carbonaceous spheres as templates to generate better light scattering among hollow spheres, improving their light harvesting capability.

Using ZnO HS as a photoanode, many types of QDs, such as single CdS, CdSe, CdTe, PbS, and PbSe; cosensitized CdS/CdSe QDs; CdS_xSe_{1-x}; and Zn_xCd_{1-x}Se alloyed QDs can be loaded for solar cell application [22–27]. Ternary alloyed QDs have drawn much attention recently because gradation composition heterostructures can be formed in order to tailor the alignment of the conduction band edges of the QDs, which is helpful to improve the electron injection efficiency [28–30]. For example, ZnO–Zn_xCd_{1-x}Se core/shell nanowire array QDSSCs form a stepwise energy alignment at the heterojunctions, where both the conduction and valence bands of the shell are either higher or lower in energy than those of the core [24,28–33], leading to a preferable transfer of electrons across the interface from Zn_xCd_{1-x}Se to ZnO. Although several types of QDSSCs based on ZnO nanostructures have been reported, it seems that the ternary alloyed QDs directly grown on ZnO hollow spheres have not been reported widely in QDSSCs' application.

In view of these backgrounds, we constructed QDSSCs based on Zn_xCd_{1-x}Se@ZnO hollow spheres (HS) with different sizes, by using a simple ion-exchange route. The strategy for the fabrication of Zn_xCd_{1-x}Se@ZnO HS is based on the difference of the solubility product constant (K_{sp}) of ZnO (6.8×10^{-17}), ZnSe (3.6×10^{-26}), and CdSe (6.31×10^{-36}) [33], implying that the pre-prepared ZnO HS can be employed as sacrificial templates to form Zn_xCd_{1-x}Se@ZnO HS by Se²⁻ anion exchange and Cd²⁺ cation exchange in sequence. Furthermore, the size of the Zn_xCd_{1-x}Se@ZnO HS could be controlled in accordance with the visible light region by using carbonaceous spherical templates, contributing to a stronger light scattering ability. To our best knowledge, the investigation of the size effect of Zn_xCd_{1-x}Se@ZnO HS on the photovoltaic performance of QDSSCs has seldom been reported. Based on experimental results, the reasons for the enhancement of the photovoltaic performance of Zn_xCd_{1-x}Se@ZnO HS QDSSCs are discussed.

2. Materials and Methods

2.1. Materials

The commercial chemical reagents, including sucrose, zinc nitrate, cadmium nitrate, selenium powder, sodium borohydride, ethylcellulose, terpinol, ethanol, sodium sulfide, and sulfur powder, were obtained from Aladdin Co. Ltd (Shanghai, China). The fluorine-doped tin oxide (FTO) conductive glass was purchased from Opvtech Co. Ltd (Yingkou, China). All of the materials were used directly without further purification.

2.2. Preparation of ZnO Hollow Microspheres

The ZnO hollow spheres (HS) were synthesized using a carbonaceous microspheres template method [34]. In a typical synthesis route, the carbonaceous microspheres, which were obtained by a hydrothermal process of a sucrose aqueous solution in a Teflon-stainless autoclave at 180 °C for 8 h (the size of carbonaceous can be modulated with different concentration of sucrose solution),

were dispersed in the 1 M aqueous solution of zinc nitrate under ultrasonic for 20 min. Then, the suspension was aged for 6 h. After aging, the suspension was filtered, washed, and dried in order to get black powders. Subsequently, the black powders were heated to 500 °C in a muffle furnace at a rate of 2 °C·min⁻¹, with holding of the temperature at 500 °C for 1 h. Finally, the resultant ZnO HS powders in white were acquired. The size of the ZnO HS can be controlled using carbonaceous microspheres with different sizes.

2.3. Construction of Zn_xCd_{1-x}Se@ZnO HS Photoanodes and QDSSCs

The ZnO HS powders (3 g), ethylcellulose (0.5 g), terpinol (10 mL), and ethanol (3 mL), were mixed together under magnetic stirring in order to form a viscous paste. The ZnO paste was doctor-bladed onto the FTO glass (2.0 × 1.5 cm). The ZnO film active area was controlled to be 0.25 cm², and the thickness of the film was tuned to be ~15 μm, using the same thickness spacers. After drying in ambient conditions, the products were annealed in a muffle furnace at 500 °C for 1 h in order to eliminate the organic residuals. The types of photoanodes constructed by different sizes of ZnO HS, including 300, 400, 500, and 800 nm, as well as a mixture of ZnO HS with different sizes (25 wt % for each size ZnO HS), were prepared for comparative investigation.

Zn_xCd_{1-x}Se@ZnO was obtained by immersing ZnO HS photoanodes in Se²⁻ and Cd²⁺ aqueous solutions, respectively. Firstly, the ZnO HS were immersed in a 0.1 M Se²⁻ ion solution prepared by reacting the Se powder with NaBH₄. The immersing process was kept at 80 °C for 12 h, and was repeated two times in order to get a desirable ZnSe thickness of ZnSe@ZnO HS. Then, the ZnSe@ZnO HS were put into a 0.1 M Cd²⁺ solution at 80 °C for 12 h; this process was also repeated two times in order to gain the final product of Zn_xCd_{1-x}Se@ZnO HS photoanodes.

For the solar cells application, the Zn_xCd_{1-x}Se@ZnO HS photoanode and Cu₂S counter electrode, which was prepared according to the previous literature [35], were assembled together by filling one drop of electrolyte consisting of 1 M S and 1 M Na₂S, in a water/methanol (1:1 in volume ratio) solution. We prepared the QDSSCs based on Zn_xCd_{1-x}Se@ZnO HS of different sizes in order for a comparative investigation of the size effect on the performance of the QDSSCs, and, moreover, three photoanodes based on a mixture of ZnO HS with different sizes (25 wt % for each size ZnO HS) were prepared under the same conditions for further investigation of the *I*-*V* performance's reproducibility.

2.4. Characterization

We employed a Quanta 450 FEG scanning electron microscopy (SEM, Hillsboro, OR, USA) and Tecnai G2 F20 transmission electron microscope (TEM, Hillsboro, TX, USA) equipped with an energy dispersive X-ray spectrometer (EDS) for elemental analysis in order to record the morphology of the prepared products. The optical absorption properties of the photoanodes were recorded using a U-3900H UV-VIS spectrophotometer (Dallas, TX, USA), which was equipped with an integrating sphere attachment for diffuse reflection measurement.

With the assistant of the Oriel *I*-*V* test station, we investigated the *I*-*V* performance of the QDSSCs. A solar simulator was used to simulate sunlight illumination with an intensity of 100 mW·cm⁻². The incident photon to the charge carrier generation efficiency (IPCE) was measured as a function of wavelength, using a 150 W Xe lamp coupled with a computer controlled monochromator.

3. Results and Discussions

The carbonaceous spheres were important for the synthesis of ZnO HS, because of their role as the template. The size controllable preparation of the carbonaceous spheres can be completed by varying the concentration of the sucrose aqueous solution. Figure 1 records the morphology changes of the resultant carbonaceous spheres as there is an increase in the sucrose concentration. The diameters of these carbonaceous spheres could be tuned from ~400 nm to ~2 μm, by simply increasing the sucrose concentration from 0.5 M to 2 M. Based on these experimental facts, we selected the carbonaceous spheres in sizes of ~400, ~600, and ~800 nm, and 1 μm, as templates. Because the scattering of

light by spherical particles may occur when the particle size is comparable to the wavelength of the incident light according to the Mie theory [19], these selected carbonaceous spheres are available for the synthesis of ZnO HS in an appropriate diameter in order to generate light scattering.

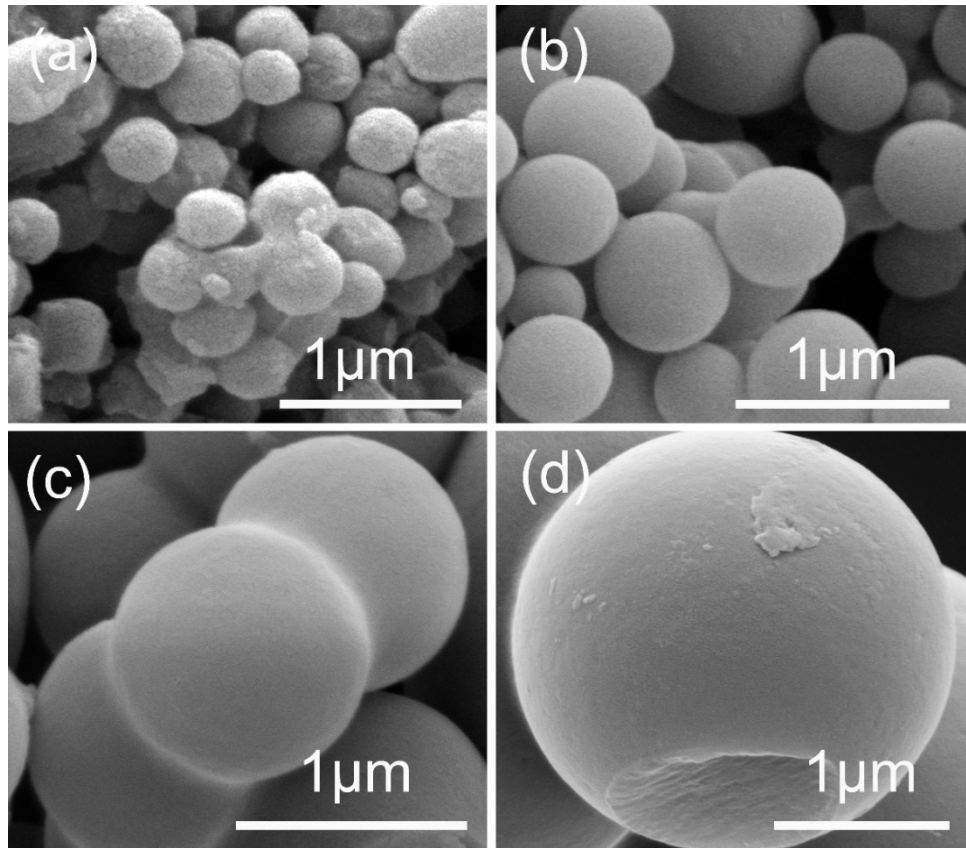


Figure 1. SEM images of carbonaceous spheres of different size prepared by varying the concentration of sucrose: (a) 0.5 M; (b) 0.75 M; (c) 1 M; (d) 2 M.

ZnO HS can be obtained using carbonaceous spheres as a template. Figure 2a shows the SEM image of the carbonaceous sphere with a size of ~ 600 nm; from one of the broken spheres, it can be seen that they are solid spheres. After the formation of ZnO HS, the surface morphology of the spheres changed to being rougher than the original carbonaceous spheres. As shown in Figure 2b, it seems that the ZnO HS is aggregated by a large number of nanoparticles. The average diameter of ZnO HS is ~ 500 nm, which is smaller than that of the carbonaceous sphere templates, demonstrating that a shrinkage of ZnO HS occurred during the heating process. This phenomenon is in accordance with previous reports [36,37]. The inset of Figure 2b provides an SEM image of a broken ZnO HS, the empty inside can be easily discerned, proved the obtained spherical structure is of hollow spheres.

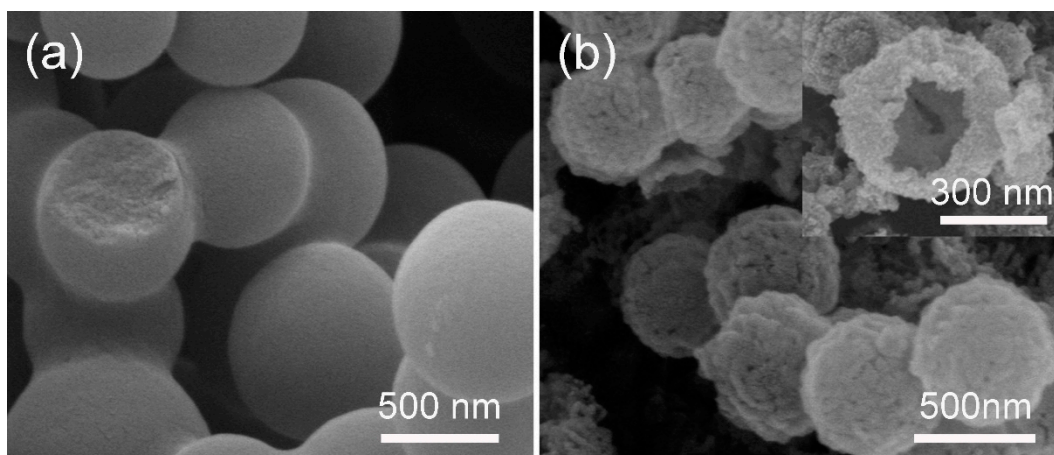


Figure 2. (a) SEM image of carbonaceous spheres template with size of ~ 600 nm; (b) ZnO hollow spheres (HS) obtained by soaking carbonaceous spheres in a 1 M zinc nitrate solution; the inset is the SEM of a broken ZnO HS.

The hollow structures of the ZnO HS were further confirmed by TEM analysis, which is presented in Figure 3a–d. Generally, all of the products show a hollow spherical structure with an identifiable shell, indicating that ZnO HS can be successfully synthesized using carbonaceous spheres as templates. Moreover, the TEM results also indicate that the size of the ZnO HS can be controlled using carbonaceous spheres with different sizes. As shown in Figure 3a–d, the sizes of the ZnO HS can be tuned from ~ 300 nm to ~ 800 nm, using different sizes of the carbonaceous templates. Figure 3e is a selective area electron diffraction (SAED) pattern of ZnO HS. The appearance of the diffraction rings indicates that the ZnO HS are in polycrystalline structure. The lattice fringes of the ZnO HS are observed using the HRTEM image in Figure 3f. By careful measurements, the lattice spacing is measured to 0.26 nm, which corresponds to the (002) plane of hexagonal ZnO (JCPDS # 36-1451).

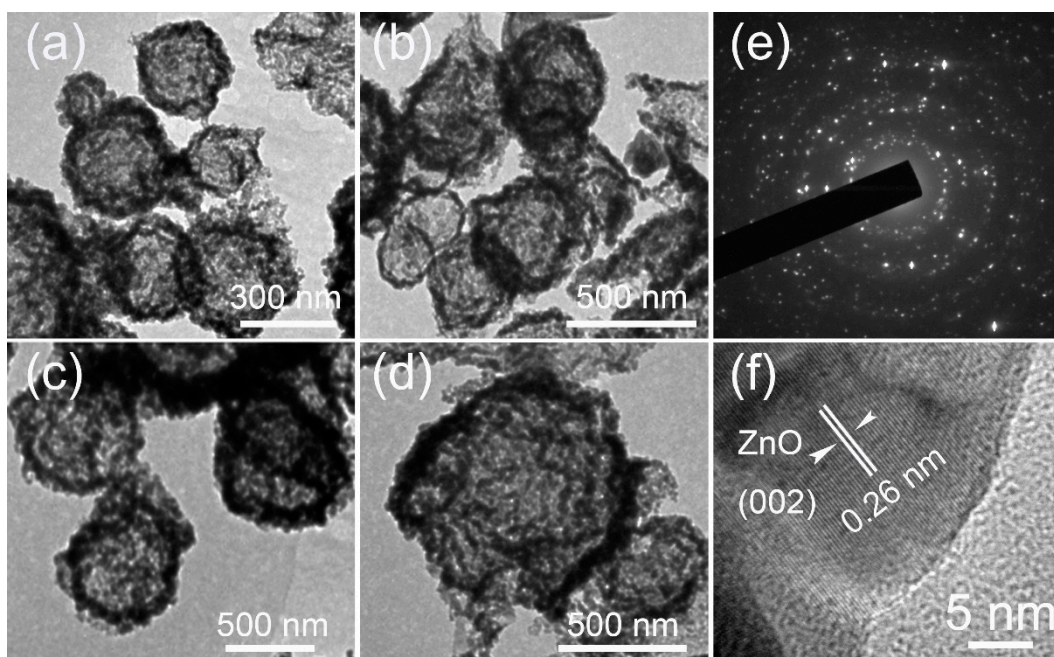


Figure 3. (a–d) TEM images of ZnO HS with a size of ~ 300 , ~ 400 , ~ 500 nm, and ~ 800 nm, respectively; (e) SAED pattern of ZnO HS; (f) the HRTEM of ZnO HS.

Based on the ZnO HS, the $Zn_xCd_{1-x}Se@ZnO$ HS were further fabricated through an ion-exchange process by soaking the ZnO HS in Se^{2-} and Cd^{2+} aqueous solutions, respectively. The morphology variation was recorded using SEM and TEM images. Figure 4a and its inset show the surface morphology of ZnO HS, and a large particles structure can be observed. The fine structure is further revealed by the TEM in Figure 4b, and the obvious shell and empty inside confirm the hollow spherical structure. The composition of the hollow sphere is shown in Figure 4c; except for the Cu element from the carbon film supported by the copper grid, only the Zn and O elements appear, and the atomic ratio is close to 1:1, confirming the formation of ZnO HS. After the ion-exchange process, a slight morphology variation on the surface of the hollow sphere is shown in Figure 4d and its inset. Smaller nanoparticles are formed on surface, indicating that a new substance has been formed on the surface of ZnO HS. In order to testify that the $Zn_xCd_{1-x}Se$ can be formed on the surface of ZnO HS, the elemental mapping test results are shown in Figure S1 (see Supplementary Materials). As is shown, the Zn, Cd, Se, and O elements can be scanned on the surface of the hollow sphere, indicating that $Zn_xCd_{1-x}Se$ has formed on the surface of ZnO after the ion-exchange process. Moreover, the TEM image in Figure 4e shows an evident morphological variation after the ion-exchange process, also implying that some new materials formed on surface of the ZnO HS. In addition, the EDS analysis of Figure 4f from a designated inner spot of the hollow sphere shell shows that after the ion-exchange process, Cd and Se elements can also be found on the inner shell, and the atomic ratio of (Zn and Cd) to (Se and O) is close to 1:1, indicating the successful formation of $Zn_xCd_{1-x}Se@ZnO$ HS.

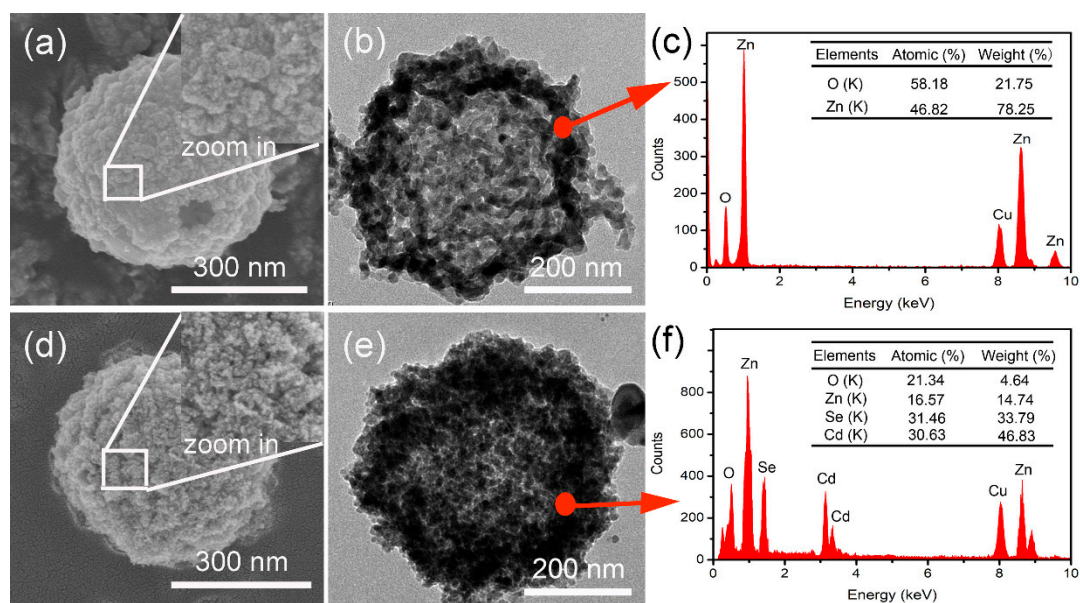


Figure 4. (a) SEM of ZnO HS, the inset is the magnified image of the selected zone; (b) TEM of ZnO HS; (c) energy dispersive X-ray spectrometer (EDS) of ZnO HS; (d) SEM of $Zn_xCd_{1-x}Se@ZnO$ HS, the inset is the magnified image of the selected zone; (e) TEM of $Zn_xCd_{1-x}Se@ZnO$ HS; (f) EDS of $Zn_xCd_{1-x}Se@ZnO$ HS.

Based on the experimental facts and TEM results, the formation mechanism of the $Zn_xCd_{1-x}Se@ZnO$ HS is proposed in Figure 5. The first important step is the use of carbonaceous spheres rich with surface carboxyl and hydroxyl functional groups, which are affinity to the Zn^{2+} ion [38] for a large amount of ion adsorption. The carbonaceous spheres are immersed in a 1 M Zn^{2+} aqueous solution for 6 h, and then taken out to be heated in air. During sintering, the carbonaceous spheres turn to CO_2 , leading to the formation of ZnO hollow spheres. The size of the ZnO hollow spheres are tuned by selecting different size of carbonaceous sphere templates. The second key step is the ion-exchange process in order to form $Zn_xCd_{1-x}Se@ZnO$ HS. A sharp difference in the solubility product constant (K_{sp}) among ZnO (6.8×10^{-17}), ZnSe (3.6×10^{-26}), and CdSe (6.1×10^{-36}) [28,33]

makes it possible for the ZnO HS to be used as sacrificial templates in order to get more stable ZnSe@ZnO HS and to further be converted into $Zn_xCd_{1-x}Se@ZnO$ HS. As illustrated in Figure 5, the ZnO hollow spheres initially conducted an anion exchange with Se^{2-} ions to form ZnSe@ZnO hollow spheres, and followed with a surface conversion of ZnSe to $Zn_xCd_{1-x}Se$ through the cation replacement of Zn^{2+} by Cd^{2+} , leading to the final $Zn_xCd_{1-x}Se@ZnO$ hollow spheres (HS).

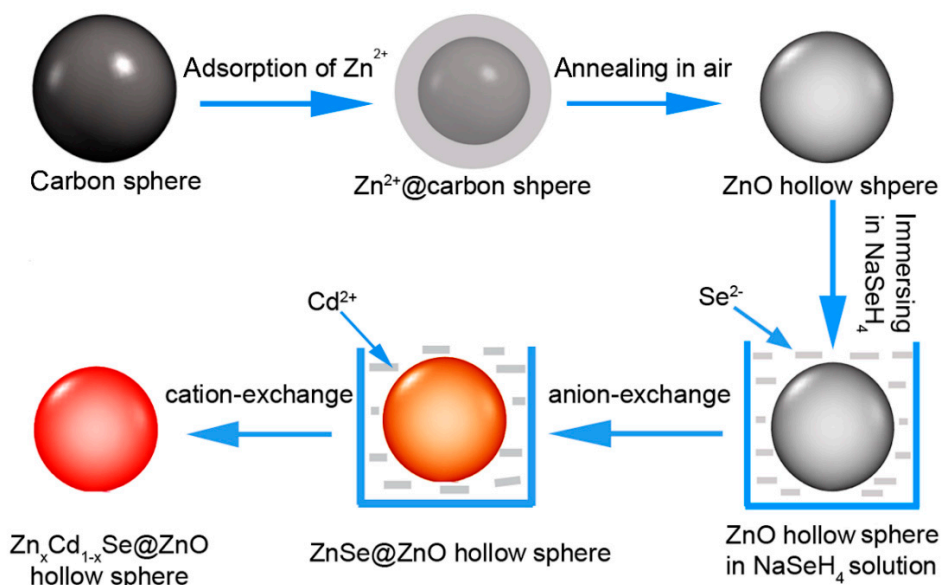


Figure 5. Illustration of the template approach to fabrication of ZnO HS and the ion-exchange process to the preparation of $Zn_xCd_{1-x}Se@ZnO$ HS.

The UV-VIS absorption spectra of the photoanodes are illustrated in Figure 6. The absorption onset of the ZnO HS centers is ~ 385 nm, corresponding to the band gap of 3.2 eV. After the anion exchange process, the absorption onset exhibits an obvious redshift to ~ 460 nm, corresponding to the band gap of 2.60 eV. This redshift phenomenon indicates that the formation of ZnSe@ZnO HS enlarges the light absorption range to the visible region. A further redshift of the absorption onset to 690 nm, which corresponds to 1.79 eV, implies the successful formation of $Zn_xCd_{1-x}Se@ZnO$ HS after the cation exchange process. The significant enlargement of the light absorption means that most of the light in the visible region can be involved in order to excite $Zn_xCd_{1-x}Se$ for the generation of electrons, providing potential application in QDSSCs.

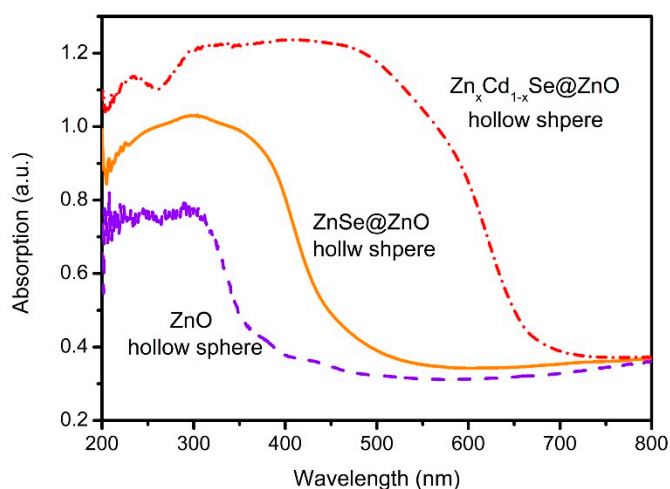


Figure 6. UV-visible absorption spectra of ZnO HS, ZnSe@ZnO HS, and $Zn_xCd_{1-x}Se@ZnO$ HS photoanodes, respectively.

As the size of the $Zn_xCd_{1-x}Se@ZnO$ HS can be controlled using carbonaceous spheres with different sizes, it is reasonable to believe that the $Zn_xCd_{1-x}Se@ZnO$ HS photoanodes will have effects on the photovoltaic performance in the QDSSCs. Figure 7a records the current density–voltage (J–V) behavior of the QDSSCs assembled with $Zn_xCd_{1-x}Se@ZnO$ HS. The $Zn_xCd_{1-x}Se@ZnO$ hollow spheres with sizes of ~300, ~400, ~500, and ~800 nm are revealed by the TEM image, as shown in Figure 7b–e. The corresponding photovoltaic parameters of these QDSSCs including short-circuit current density (J_{sc}), open-circuit voltage (V_{oc}), fill factor (FF), and power conversion efficiency (PCE), are also summarized in Table 1.

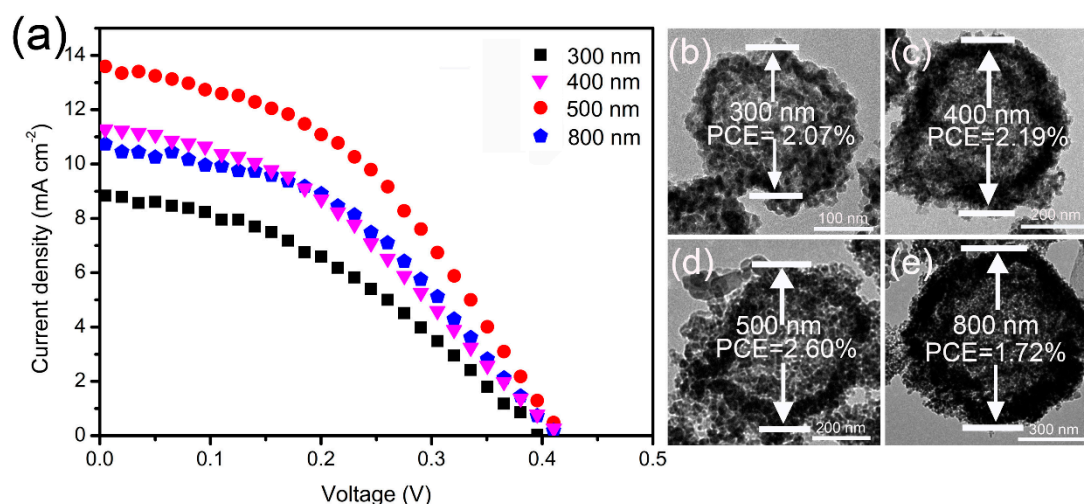


Figure 7. (a) Current density–voltage (J–V) curves of quantum dot sensitized solar cells (QDSSCs) based on $Zn_xCd_{1-x}Se@ZnO$ HS with a size of 300, 400, 500, and 800 nm; (b–e) the corresponding TEM images of $Zn_xCd_{1-x}Se@ZnO$ HS in different sizes with their power conversion efficiency (PCE).

Table 1. Size influence of $Zn_xCd_{1-x}Se@ZnO$ hollow spheres (HS) on photovoltaic performance. FF—fill factor; PCE—power conversion efficiency.

Size (nm)	J_{sc} ($\text{mA}\cdot\text{cm}^{-2}$)	V_{oc} (V)	FF	PCE (%)
~300	11.30	0.42	0.44	2.07
~400	11.61	0.41	0.46	2.19
~500	13.46	0.42	0.46	2.60
~800	8.79	0.40	0.49	1.72

The QDSSC based on the ~300 nm $Zn_xCd_{1-x}Se@ZnO$ HS photoanode exhibit a J_{sc} of $11.30 \text{ mA}\cdot\text{cm}^{-2}$, a V_{oc} of 0.42 V, and a FF of 0.44, producing a PCE of 2.07%. As the size of the $Zn_xCd_{1-x}Se@ZnO$ HS increases to ~400 nm, the QDSSC shows a J_{sc} of $11.61 \text{ mA}\cdot\text{cm}^{-2}$, a V_{oc} of 0.41 V, and a FF of 0.46, leading to an increase in PCE to 2.19%. A higher PCE of QDSSC is acquired by ~500 nm $Zn_xCd_{1-x}Se@ZnO$ HS, which presents a J_{sc} of $13.46 \text{ mA}\cdot\text{cm}^{-2}$, a V_{oc} of 0.42 V, a FF of 0.46, yielding the highest PCE of 2.60% among these sample QDSSCs. However, further increasing the $Zn_xCd_{1-x}Se@ZnO$ HS to ~800 nm leads to a decrease of PCE to 1.72%, with J_{sc} of $8.79 \text{ mA}\cdot\text{cm}^{-2}$, V_{oc} of 0.40 V, and FF of 0.49. Apparently, the only difference among these sample QDSSCs is the size of the $Zn_xCd_{1-x}Se@ZnO$ HS. Therefore, we believe that a size effect of the $Zn_xCd_{1-x}Se@ZnO$ hollow spheres would probably be responsible for the changes of the photovoltaic performance.

The explanations for the photovoltaic performance variation related to the structure of the $Zn_xCd_{1-x}Se@ZnO$ HS can be illustrated in Figure 8. According to the J–V curves results (Figure 7), it can be concluded that the change of J_{sc} among these $Zn_xCd_{1-x}Se@ZnO$ solar cells is the main reason for the difference in the photovoltaic performance. We believe that three factors, including light scattering on the surface of the hollow spheres, light reflection in the hollow spheres, and a band edges realignment caused by the gradient $Zn_xCd_{1-x}Se@ZnO$ structure, have influence on the variation

of J_{sc} . Figure 8a gives the working principle of QDSSC based on the $Zn_xCd_{1-x}Se@ZnO$ photoanode. Under illumination, the $Zn_xCd_{1-x}Se@ZnO$ will be excited so as to generate electrons. More light being absorbed will produce more electrons favorable to the increase of J_{sc} . However, a significant portion of the light emitted on the photoanodes would transmit through the photoanode, without interacting with the $Zn_xCd_{1-x}Se@ZnO$ HS because of the smaller size hollow spheres. The resonant scattering of light is anticipated to occur for spherical particles in a size comparable to the incident light, according to the Mie theory and the Anderson localization of light [39]. In our case, the photoanode is packed by the $Zn_xCd_{1-x}Se@ZnO$ HS, by controlling the size of the hollow spheres, ~ 500 nm $Zn_xCd_{1-x}Se@ZnO$ HS is in the range of visible light, which results in a stronger scattering effect among the $Zn_xCd_{1-x}Se@ZnO$ hollow spheres than other sized hollow spheres, providing the photons more chances to be absorbed, and eventually leading to an enhanced light harvesting efficiency. In addition, the hollow spheres structure of $Zn_xCd_{1-x}Se@ZnO$ allows for light to be reflected by many times when it encounters the shell of the hollow sphere, because of its curved surface, as shown in Figure 8b, also leading to the enhancement of the light harvesting efficiency.

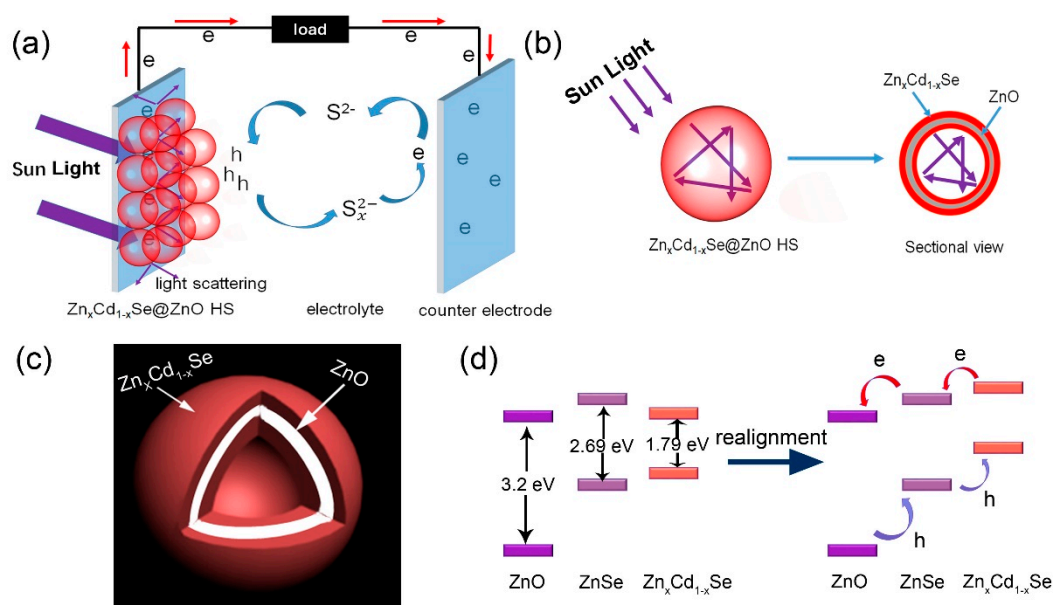


Figure 8. (a) The model of the QDSSC based on the $Zn_xCd_{1-x}Se@ZnO$ photoanode; (b) the light pathway inside the $Zn_xCd_{1-x}Se@ZnO$ HS; (c) the composition gradient structural model of $Zn_xCd_{1-x}Se@ZnO$ HS; (d) band edges realignment in $Zn_xCd_{1-x}Se@ZnO$ HS.

A sandwich composition gradient structure of $Zn_xCd_{1-x}Se@ZnO$ would be formed on the shell of the hollow spheres because of the ion-exchange process, as illustrated in Figure 8c. The ZnSe layer is firstly formed on the ZnO HS surface during the Se^{2-} ion-exchange process, then, a Cd^{2+} ion-exchange process replaced the Zn^{2+} from the surface of the ZnSe layer, forming a sandwich composition gradient structure of $Zn_xCd_{1-x}Se@ZnO$ HS with a Cd^{2+} rich in surface [22,33]. This sandwich structure caused a band realignment, as shown in Figure 8d. When the $Zn_xCd_{1-x}Se@ZnO$ formed, the ZnO, ZnSe, and $Zn_xCd_{1-x}Se$ were brought into contact closely, and the energy level difference between ZnSe and $Zn_xCd_{1-x}Se$ would cause an electron flow from ZnSe to $Zn_xCd_{1-x}Se$, which is known as the Fermi level alignment, triggering a downward and upward shift of band edges of ZnSe and $Zn_xCd_{1-x}Se$, respectively [32]. The formation of a stepwise conduction band edge alignment in the order of $Zn_xCd_{1-x}Se > ZnSe > ZnO$ for a sandwich composition gradient $Zn_xCd_{1-x}Se@ZnO$ HS is beneficial for enhancing the injection and collection of photoexcited electrons to the conduction band of the ZnO layer.

The IPCE spectra of the QDSSCs based on the $Zn_xCd_{1-x}Se@ZnO$ HS with different sizes can provide more information on the enhancement of J_{sc} . As seen in Figure 9, two interesting observations

can be identified when comparing these spectra. The first one is that the range of the photoresponse centers is in the visible light region for all of the sample solar cells, demonstrating the excitation of $Zn_xCd_{1-x}Se$ as the primary event responsible for photocurrent generation. The second is a considerable increase of IPCE with the increasing size of $Zn_xCd_{1-x}Se@ZnO$ HS in the visible light region, especially the highest IPCE value produced by ~ 500 nm $Zn_xCd_{1-x}Se@ZnO$ HS. Considering its size in the range of the visible light region, its IPCE enhancement is mainly attributed to the increase of light scattering, contributing eventually to the improvement of J_{sc} .

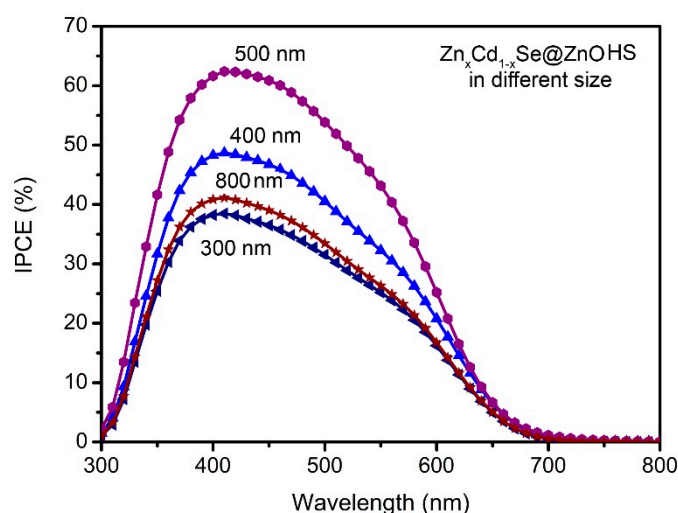


Figure 9. The incident photo-to-current conversion efficiency (IPCE) spectra of QDSSCs based on $Zn_xCd_{1-x}Se@ZnO$ HS in the sizes of ~ 300 , ~ 400 , ~ 500 , and ~ 800 nm, respectively.

According to the above discussion, a ~ 500 nm $Zn_xCd_{1-x}Se@ZnO$ HS shows better scattering of light in the visible light region than the other HS sizes. However, the single size distribution of the hollow spheres seems to not take full use of the visible light region in order to generate light scattering. Therefore, the photoanode constructed by a mixture of ZnO HS with different sizes from 300 to 800 nm was fabricated, and its photovoltaic performance is shown in Figure 10. As the J–V curves are shown in Figure 10a, and the mixture of the hollow spheres with different sizes can further improve the J_{sc} to $20.77 \text{ mA}\cdot\text{cm}^{-2}$, leading to the enhancement of PCE to 2.95%. In order to guarantee the performance's reproducibility of our QDSSC based on ZnO HS with different sizes from 300 nm to 800 nm, we also prepared three QDSSCs under the same conditions for the J–V test, in order to investigate the stability of the photoanodes. The compared J–V test results are shown in Figure S2 in the Supplementary Materials, which shows a relative stable variation PCE performance (from 3.05% to 2.92%). In comparison with a previous report, our QDSSC's J_{sc} and PCE outperformed the similar $ZnO-Zn_xCd_{1-x}Se$ QDSSC based on ZnO nanowire arrays ($J_{sc} = 6.7 \text{ mA}\cdot\text{cm}^{-2}$, $V_{oc} = 0.64 \text{ V}$, $FF = 0.35$, $PCE = 1.5\%$) [32], indicating this kind of structure's potential advantages in improving the J_{sc} of solar cells. The IPCE in Figure 10b shows that the maximum IPCE value can reach to 85%, indicating a better utilization of the visible light region in order to enhance the light harvesting efficiency. This significant improvement of the photovoltaic performance using a mixture of hollow spheres can be ascribed to the enhanced light scattering in the different wavelengths of light caused by the wide range of sizes, from 300 to 800 nm, as shown in Figure 10c, compared with the single size of the hollow spheres, indicating the potential application of this strategy for designing QDSSCs.

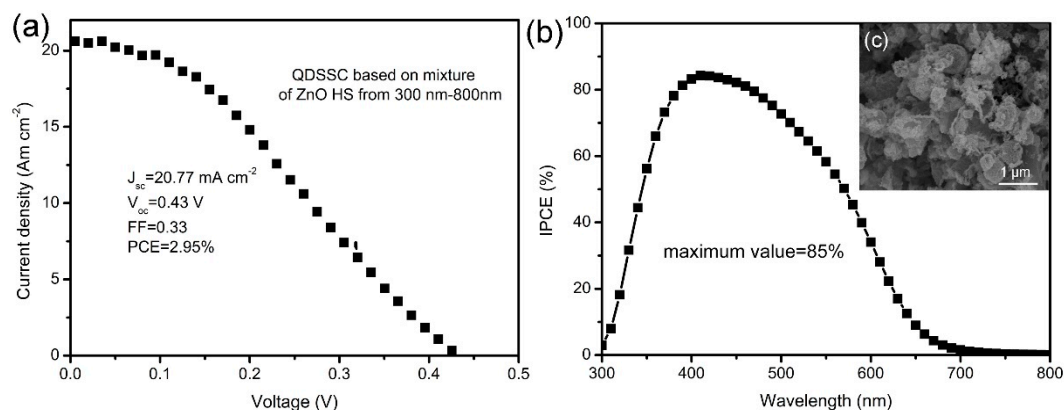


Figure 10. (a) The J–V curve of QDSSC based on a mixture of ZnO HS in different sizes, from 300–800 nm; (b) the corresponding IPCE spectrum; (c) the SEM image of the corresponding photoanode.

4. Conclusions

In summary, unique $Zn_xCd_{1-x}Se@ZnO$ hollow spheres (HS) with a gradient position are successfully fabricated by an ion-exchange process with assistance from carbonaceous spheres as the template. The size of the $Zn_xCd_{1-x}Se@ZnO$ hollow spheres can be controlled by using carbonaceous spheres of different sizes. The influence on QDSSCs caused by the size variations of the $Zn_xCd_{1-x}Se@ZnO$ hollow spheres was investigated. Light scattering and the composition gradient structure of $Zn_xCd_{1-x}Se@ZnO$ hollow spheres are responsible for the enhancement of the photovoltaic performance. The size of the $Zn_xCd_{1-x}Se@ZnO$ hollow spheres at ~500 nm shows a better effect than the other sizes of the hollow spheres. By using a mixture of hollow spheres, with different sizes from 300 nm to 800 nm, the PCE of the QDSSC can be improved to 2.95%, showing the feasibility of the $Zn_xCd_{1-x}Se@ZnO$ hollow spheres in the design of high efficient QDSSCs.

Supplementary Materials: The following are available online at <http://www.mdpi.com/2079-4991/9/2/132/s1>, Figure S1: (a) SEM image $Zn_xCd_{1-x}Se@ZnO$ hollow sphere, (b–e) elemental mapping of $Zn_xCd_{1-x}Se@ZnO$ hollow sphere, Figure S2: J–V curves QDSSCs based on mixture of ZnO HS from 300 nm to 800 nm (three QDSSCs are repeatedly prepared with same conditions for comparisons and reproducibility check).

Author Contributions: Methodology, Validation, Analysis and Writing—Original Draft Preparation, L.Y.; Conceptualization, Resources, Supervision, Project Administration, and Writing—Review & Editing, Z.L.

Funding: This research was funded by the National Natural Science Foundation of China (grant number 51862007), the Natural Science Foundation of Gansu Province (grant number 18JR3RG210), and the University Research Project of Gansu Province (grant number 2018A-091).

Conflicts of Interest: The authors declare no conflict of interest.

References

- Lu, Y.B.; Li, L.; Su, S.C.; Chen, Y.L.; Song, Y.L.; Jiao, S.J. A novel TiO_2 nanostructure as photoanode for highly efficient CdSe quantum dot-sensitized solar cells. *RSC Adv.* **2017**, *7*, 9795–9802. [CrossRef]
- Li, Z.; Yu, L.; Liu, Y.; Sun, S. Efficient quantum dot-sensitized solar cell based on $CdS_xSe_{1-x}/Mn-CdS/TiO_2$ nanotube array electrode. *Electrochim. Acta* **2015**, *153*, 200–209. [CrossRef]
- Peng, Z.; Chen, X.; Liu, Y.; Chen, J.; Chen, J. Balance on the charge generation, separation and transfer performance of different TiO_2 nanostructures in quantum dot sensitized solar cells. *Mater. Res. Bull.* **2017**, *94*, 463–471. [CrossRef]
- Grätzel, M. Photoelectrochemical cells. *Nature* **2001**, *414*, 338–344. [CrossRef]
- Green, M.A.; Ho-Baillie, A.; Snaith, H.J. The emergence of perovskite solar cells. *Nat. Photonics* **2014**, *8*, 506–514. [CrossRef]
- Tian, J.; Cao, G. Semiconductor quantum dot-sensitized solar cells. *Nano Rev.* **2013**, *4*, 22578. [CrossRef] [PubMed]

7. Hori, K.; Zhang, Y.; Tusamalee, P.; Nakazawa, N.; Yoshihara, Y.; Wang, R.; Toyoda, T.; Hayase, S.; Shen, Q. Interface passivation effects on photovoltaic performance of quantum dot sensitized inverse opal TiO₂ solar cells. *Nanomaterials* **2018**, *8*, 460. [[CrossRef](#)]
8. Ruhle, S.; Shalom, M.; Zaban, A. Quantum-dot-sensitized solar cells. *Chemphyschem* **2010**, *11*, 2290–2304. [[CrossRef](#)] [[PubMed](#)]
9. Choi, H.; Nahm, C.; Kim, J.; Kim, C.; Kang, S.; Hwang, T.; Park, B. Review paper: Toward highly efficient quantum-dot- and dye-sensitized solar cells. *Curr. Appl. Phys.* **2013**, *13*, S2–S13. [[CrossRef](#)]
10. Li, G.; Sheng, L.; Hu, J.; Li, P.; Wang, K. Engineering flexible dye-sensitized solar cells for portable electronics. *Sol. Energy* **2019**, *177*, 80–98. [[CrossRef](#)]
11. Sacco, A.; Bella, F.; Pierre, S.D.L.; Catellino, M.; Bainco, S.; Bongiovanni, R.; Pirri, C.F. Electrodes/electrolyte interfaces in the presence of a surface-modified photopolymer electrolyte: Application in dye-sensitized solar cells. *ChemPhysChem* **2015**, *16*, 960–969. [[CrossRef](#)] [[PubMed](#)]
12. Bella, F.; Sacco, A.; Salvador, G.P.; Bianco, S.; Tresso, E.; Pirri, C.F.; Bongiovanni, R. First Pseudohalogen polymer electrolyte for dye-sensitized solar cells promising for in situ photopolymerization. *J. Phys. Chem. C* **2013**, *117*, 20421–20430. [[CrossRef](#)]
13. Bella, F.; Imperiyka, M.; Ahmad, A. Photochemically produced quasi-linear copolymers for stable and efficient electrolytes in dye-sensitized solar cells. *J. Photochem. Photobiol. A Chem.* **2014**, *289*, 73–80. [[CrossRef](#)]
14. Wang, W.; Feng, W.; Du, J.; Xue, W.; Zhang, L.; Zhao, L.; Li, Y.; Zhong, X. Cosensitized quantum dot solar cells with conversion efficiency over 12%. *Adv. Mater.* **2018**, *30*, 1705746. [[CrossRef](#)] [[PubMed](#)]
15. Du, J.; Du, Z.; Hu, J.S.; Pan, Z.; Shen, Q.; Sun, J.; Long, D.; Dong, H.; Sun, L.; Zhong, X.; et al. Zn-Cu-In-Se quantum dot solar cells with a certified power conversion efficiency of 11.6%. *J. Am. Chem. Soc.* **2016**, *138*, 4201–4209. [[CrossRef](#)] [[PubMed](#)]
16. Shen, G.; Du, Z.; Pan, Z.; Du, J.; Zhong, X. Solar paint from TiO₂ particles supported quantum dots for photoanodes in quantum dot-sensitized solar cells. *ACS Omega* **2018**, *3*, 1102–1109. [[CrossRef](#)]
17. Sahu, A.; Chaurashiya, R.; Hiremath, K.; Dixit, A. Nanostructured zinc titanate wide band gap semiconductor as a photoelectrode material for quantum dot sensitized solar cells. *Sol. Energy* **2018**, *163*, 338–346. [[CrossRef](#)]
18. Wen, S.; Li, M.; Yang, J.; Mei, X.; Wu, B.; Liu, X.; Heng, J.; Qin, D.; Hou, L.; Wang, D. Rationally controlled synthesis of Cd_{1-x}Se_xTe_{1-x} alloy nanocrystals and their application in efficient graded band gap solar cells. *Nanomaterials* **2017**, *7*, 380. [[CrossRef](#)]
19. Xi, J.; Zhang, Q.; Park, K.; Sun, Y.; Cao, G. Enhanced power conversion efficiency in dye-sensitized solar cells with TiO₂ aggregates/nanocrystallites mixed photoelectrodes. *Electrochim. Acta* **2011**, *56*, 1960–1966. [[CrossRef](#)]
20. Zhang, Q.; Chou, T.P.; Russo, B.; Jenekhe, S.A.; Cao, G. Aggregation of ZnO nanocrystallites for high conversion efficiency in dye-sensitized solar cells. *Angew. Chem. Int. Ed. Engl.* **2008**, *47*, 2402–2406. [[CrossRef](#)]
21. Titirici, M.M.; Antonietti, M.; Thomas, A. A Generalized synthesis of metal oxide hollow spheres using a hydrothermal approach. *Chem. Mater.* **2006**, *18*, 3808–3812. [[CrossRef](#)]
22. Li, H.; Cheng, C.; Li, X.; Liu, J.; Guan, C.; Tay, Y.Y.; Fan, H.J. Composition-graded Zn_xCd_{1-x}Se@ZnO core-shell nanowire array electrodes for photoelectrochemical hydrogen generation. *J. Phys. Chem. C* **2012**, *116*, 3802–3807. [[CrossRef](#)]
23. Gertman, R.; Osherov, A.; Golan, Y.; Visoly-Fisher, I. Chemical bath deposited PbS thin films on ZnO nanowires for photovoltaic applications. *Thin Solid Films* **2014**, *550*, 149–155. [[CrossRef](#)]
24. Justin Raj, C.; Karthick, S.N.; Park, S.; Hemalatha, K.V.; Kim, S.K.; Prabakar, K.; Kim, H.J. Improved photovoltaic performance of CdSe/CdS/PbS quantum dot sensitized ZnO nanorod array solar cell. *J. Power Sources* **2014**, *248*, 439–446. [[CrossRef](#)]
25. Hou, J.; Zhao, H.; Huang, F.; Jing, Q.; Cao, H.; Wu, Q.; Peng, S.; Cao, G. High performance of Mn-doped CdSe quantum dot sensitized solar cells based on the vertical ZnO nanorod arrays. *J. Power Sources* **2016**, *325*, 438–445. [[CrossRef](#)]
26. Zervos, M.; Vasile, E.; Vasile, E.; Othonos, A. Core-shell PbS/Sn:In₂O₃ and branched PbIn₂S₄/Sn:In₂O₃ nanowires in quantum dot sensitized solar cells. *Nanotechnology* **2017**, *28*, 054004. [[CrossRef](#)] [[PubMed](#)]
27. Liu, H.; Zhang, G.; Yin, J.; Liang, J.; Sun, W.; Shen, Z. Fabrication of ZnO nanostructures sensitized with CdS quantum dots for photovoltaic application using a convenient solution method. *Mater. Res. Bull.* **2015**, *61*, 492–498. [[CrossRef](#)]

28. Li, Z.; Yu, L.; Liu, Y.; Sun, S. Arrays of $Zn_xCd_{1-x}Se/TiO_2$ nanotubes: Fabrication by ion-exchange and photovoltaic applications. *J. Mater. Sci. Mater. Electron.* **2015**, *26*, 1625–1633. [[CrossRef](#)]
29. Zhou, R.; Wan, L.; Niu, H.; Yang, L.; Mao, X.; Zhang, Q.; Miao, S.; Xu, J.; Cao, G. Tailoring band structure of ternary CdS_xSe_{1-x} quantum dots for highly efficient sensitized solar cells. *Sol. Energy Mater. Sol. Cells* **2016**, *155*, 20–29. [[CrossRef](#)]
30. Jiang, T.; Shen, M.; Dai, P.; Wu, M.; Yu, X.; Li, G.; Xu, X.; Zeng, H. Cd-free Cu-Zn-In-S/ZnS quantum dots@ SiO_2 multiple cores nanostructure: Preparation and application for white LEDs. *Nanotechnology* **2017**, *28*, 435702. [[CrossRef](#)]
31. Xu, J.; Yang, X.; Yang, Q.D.; Wong, T.L.; Lee, S.T.; Zhang, W.J.; Lee, C.S. Arrays of CdSe sensitized ZnO/ZnSe nanocables for efficient solar cells with high open-circuit voltage. *J. Mater. Chem.* **2012**, *22*, 13374. [[CrossRef](#)]
32. Myung, Y.; Kang, J.H.; Choi, J.W.; Jang, D.M.; Park, J. Polytypic ZnCdSe shell layer on a ZnO nanowire array for enhanced solar cell efficiency. *J. Mater. Chem.* **2012**, *22*, 2157–2165. [[CrossRef](#)]
33. Xu, J.; Yang, X.; Wang, H.; Chen, X.; Luan, C.; Xu, Z.; Lu, Z.; Roy, V.A.; Zhang, W.; Lee, C.S. Arrays of ZnO/ $Zn_xCd_{1-x}Se$ nanocables: Band gap engineering and photovoltaic applications. *Nano Lett.* **2011**, *11*, 4138–4143. [[CrossRef](#)] [[PubMed](#)]
34. Dong, Z.; Lai, X.; Halpert, J.E.; Yang, N.; Yi, L.; Zhai, J.; Wang, D.; Tang, Z.; Jiang, L. Accurate control of multishelled ZnO hollow microspheres for dye-sensitized solar cells with high efficiency. *Adv. Mater.* **2012**, *24*, 1046–1049. [[CrossRef](#)] [[PubMed](#)]
35. Kalanur, S.S.; Chae, S.Y.; Joo, O.S. Transparent $Cu_{1.8}S$ and CuS thin films on FTO as efficient counter electrode for quantum dot solar cells. *Electrochim. Acta* **2013**, *103*, 91–95. [[CrossRef](#)]
36. Wang, X.; Hu, P.; Fangli, Y.; Yu, L. Preparation and characterization of ZnO hollow spheres and ZnO-carbon composite materials using colloidal carbon spheres as templates. *J. Phys. Chem. C* **2007**, *111*, 6706–6712. [[CrossRef](#)]
37. Lai, X.; Li, J.; Korgel, B.A.; Dong, Z.; Li, Z.; Su, F.; Du, J.; Wang, D. General synthesis and gas-sensing properties of multiple-shell metal oxide hollow microspheres. *Angew. Chem. Int. Ed. Engl.* **2011**, *50*, 2738–2741. [[CrossRef](#)]
38. Lai, X.; Halpert, J.E.; Wang, D. Recent advances in micro-/nano-structured hollow spheres for energy applications: From simple to complex systems. *Energy Environ. Sci.* **2012**, *5*, 5604–5618. [[CrossRef](#)]
39. Zhou, R.; Zhang, Q.; Uchaker, E.; Lan, J.; Yin, M.; Cao, G. Mesoporous TiO_2 beads for high efficiency CdS/CdSe quantum dot co-sensitized solar cells. *J. Mater. Chem. A* **2014**, *2*, 2517–2525. [[CrossRef](#)]



© 2019 by the authors. Licensee MDPI, Basel, Switzerland. This article is an open access article distributed under the terms and conditions of the Creative Commons Attribution (CC BY) license (<http://creativecommons.org/licenses/by/4.0/>).